

Control of Multi-level Voltage States in a Hysteretic SQUID Ring-Resonator System

P. Stiehl, M. J. Everitt, and T. D. Clark

School of Science and Technology, University of Sussex, Brighton, Sussex, BN1 9QT, U.K.

J. F. Ralph

Department of Electrical Engineering and Electronics,
University of Liverpool, Brownlow Hill, Liverpool, L69 3GJ, U.K.

In this paper we study numerical solutions to the quasi-classical equations of motion for a SQUID ring-radio frequency (rf) resonator system in the regime where the ring is highly hysteretic. In line with experiment, we show that for a suitable choice of ring circuit parameters the solutions to these equations of motion comprise sets of levels in the rf voltage-current dynamics of the coupled system. We further demonstrate that transitions, both up and down, between these levels can be controlled by voltage pulses applied to the system, thus opening up the possibility of high order (e.g. 10 state), multi-level logic and memory.

I. INTRODUCTION

In an earlier paper [1] we reported on a new phenomena generated by the non-linear interaction of a SQUID ring (here, a single Josephson weak link enclosed by a thick superconducting ring) with a parallel LC resonant (tank) circuit. The block diagram for this coupled system is shown in figure 1. As has now become apparent, SQUID rings can display behaviour ranging from fully quantum mechanical [2, 3, 4, 5] through to quasi-classical [6, 7, 8, 9] depending on the circuit parameters of the ring and the temperature (T) of the environment. At temperatures of a few K, and for relatively large weak link capacitances 10^{12} – 10^{13} F, it is well established [6, 8] that a SQUID ring (inductance L_s , weak link critical current I_c) can be treated quasi-classically, i.e. as a particle moving, with damping, in a cosine modulated parabolic potential,

$$U(\phi; \Phi_x) = \frac{(\phi_s - \phi_x)^2}{2} - \frac{I_c \phi_0}{2} \cos \frac{2\phi_s}{\phi_0} \quad (1)$$

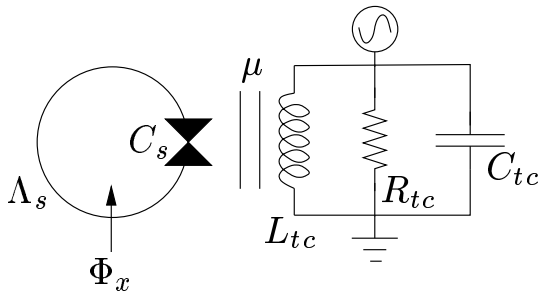


FIG. 1: Block diagram for an inductively coupled SQUID ring-tank circuit system together with excitation, static bias and readout circuitry.

where ϕ_x is the external magnetic flux applied to the ring, ϕ_s is the total included flux in the ring and $\phi_0 = h/2e$ is the superconducting flux quantum. In this quasi-classical regime it is usual practice to describe the SQUID ring, and its interactions, using the Resistively Shunted Junction plus Capacitance (RSJ+C) model [8, 10]. Here, we denote the ring weak link effective capacitance by C_s and the parallel link resistance by R_s . Furthermore, in making use of this model it is convenient to introduce the β -parameter for the SQUID ring, $\beta = 2\pi I_c \phi_0 / \Phi_0$. This allows us to distinguish between the parameter space in which I_c is always a single-valued function of ϕ_x (the inductive regime) and the hysteretic regime where I_c can be multi-valued in ϕ_x [8, 10].

The cosine in the potential (1) leads to a superconducting screening current response in the SQUID ring which is manifestly a non-linear, and ϕ_0 -periodic, function of ϕ_s . When at least part of this external flux is time dependent, and applied through an inductively coupled resonant circuit, the ring-resonator system displays non-linear dynamical behaviour which has been the focus of much research over the last three decades [6, 7, 11]. It is precisely this behaviour that forms the basis of the well known ac-biased SQUID magnetometer [8, 10, 12]. Although not invariably the case, it has been common practice [12] to make use of a radio frequency (rf ~ 20 MHz), parallel LC (tank circuit) resonator in these coupled magnetometer systems. In the work described here we adopt this frequency regime for the resonant circuit. Considered on its own, of course, the tank circuit circuit is strictly linear, i.e. on resonance the rf voltage (V_{out}) across it is linearly dependent on the level of rf drive input current ($I_{in}(t)$) applied. However, when a SQUID ring is coupled to such a tank circuit the situation can alter radically. With the SQUID ring potential above, and at finite critical current I_c , the screening supercurrent $I_s = I_c \sin \phi_s$ owing in the ring to oppose any externally applied flux ϕ_x is a non-linear function of this flux. Since both the SQUID ring and the tank circuit are microscopic in nature, the back reaction through the inductive coupling leads to the

system displaying non-linear, even chaotic, dynamics. In general the stronger the non-linearity in $I_s(x)$, the more pronounced the non-linear behaviour can be. This non-linear behaviour is most easily seen in plots of V_{out} versus $I_{in}(t)$, these also being dependent on the level of static or quasi-static bias $\mu(x)$ applied to the SQUID ring. In SQUID magnetometer systems these characteristics

display essentially constant rf voltage steps in the (time averaged) V_{out} versus $I_{in}(t)$ at intervals periodic in I_{in} . These SQUID steps are modulated in a ϕ_0 -periodic manner by the external bias $\mu(x)$ [8, 12, 13]. The ring-tank circuit system is described dynamically by two (coupled) equations of motion, one for the tank circuit and the other for the ring. These are given by

$$C_{tc} \frac{d^2 \phi_{tc}}{dt^2} + \frac{1}{R_{tc}} \frac{d \phi_{tc}}{dt} + \frac{\phi_{tc}}{L_{tc} (1 - K^2)} = I_{in}(t) + \frac{\phi_s}{(1 - K^2)} \quad (\text{Tank circuit}) \quad (2)$$

$$C_s \frac{d^2 \phi_s}{dt^2} + \frac{1}{R_s} \frac{d \phi_s}{dt} + I_c \sin \frac{2 \phi_s}{\phi_0} + \frac{\phi_s}{(1 - K^2)} = \frac{\phi_{tc}}{(1 - K^2)} \quad (\text{SQUID ring}) \quad (3)$$

where the subscripts tc and s refer, respectively, to the tank circuit and the SQUID ring and $K = M/L_{tc}$ is the fraction of the flux coupled between the ring and the tank circuit. Thus, C_{tc} and L_{tc} are, respectively, the tank circuit capacitance and inductance, ϕ_{tc} is the flux in the tank circuit inductor, R_{tc} is the resistance of the parallel tank circuit on resonance and $K = \frac{M}{\sqrt{L_{tc} L_s}}$ quantifies the strength of the inductive coupling between the ring and tank circuit with a mutual inductance of M . In (2) and (3) the last terms on the right hand sides of these equations describe the back reaction between the ring and the tank circuit.

In the original paper [1] we used (2) and (3) to compute the V_{out} versus I_{in} dynamics of the ring-tank circuit system in the highly hysteretic, strongly underdamped, regime to model the observed experimental behaviour. What was recorded experimentally was a succession of plateau regions in the time averaged V_{out} versus I_{in} characteristics of the ring-tank circuit system. Each plateau region consisted of a set of parallel steps at regular separations along the I_{in} axis. The lengths of these steps along this axis were much greater than those observed in standard hysteretic SQUID magnetometer characteristics, where, typically, a few [8, 12]. In addition, for each individual plateau the rf voltage (V_{out}) at which these steps occurred varied ϕ_0 -periodically in I_{in} . In experiment [1] the ring-tank circuit system was observed to jump stochastically [14, 15, 16] between the various steps associated with each plateau. Since, in practice, it was easy experimentally to access circuit parameters in which many steps per plateau region could be seen (a maximum of 19 steps/plateau was recorded over the course of these experiments), there seemed a possibility that the plateaux and steps could be utilised to create multi-level logic as an alternative to the standard binary logic. We found that with simulated low temperature noise on the tank circuit drive current, introduced via a noise distribution for a thermal bath, the solutions to these coupled equations of motion modelled our experimental results

very well, including the stochastic jumping between steps on particular plateaux. We argued in the paper [1] that when the SQUID ring is sufficiently underdamped it no longer follows the potential (1) adiabatically as the rf flux coupled in from the tank circuit changes with time. Essentially, it is this non-adiabatic response that generates the large multi-step plateaux in the ring-tank circuit V_{out} versus I_{in} characteristics, each step corresponding to a different flux jump trajectory (local well to local well) in (1). Nevertheless, even though we had demonstrated that the underdamped RSJ+C description could model the experimentally observed plateaux and steps, the stochastic jumping between steps generated in the theoretical calculations required more explanation. In the experiments we took the view, we believed quite validly, that these jumping processes were caused by ambient noise. However, for technical reasons we were not able to measure the full spectral density function of this noise and with the computer power then available to us we could not be certain that the stochastic jumping processes seen in the simulations did not arise because of computational inaccuracies. New calculations, at much higher accuracy, are the basis of the work reported here. At this new level we have been able to show that, from the viewpoint of the simulations presented in our previous paper [1], the jumping processes arose due to the build up of computational error in the numerical integration for the evolution of the system. Repeating the calculations, and eliminating this potential problem by using more accurate integration methods, only single steps are generated in each plateau region, even with large variance current noise added. Nevertheless, it was clear from experiment that the ring-tank circuit system could be perturbed to generate jumps. We now show how this can be achieved in a controlled way, pointing to possible device applications in multi-level logic.

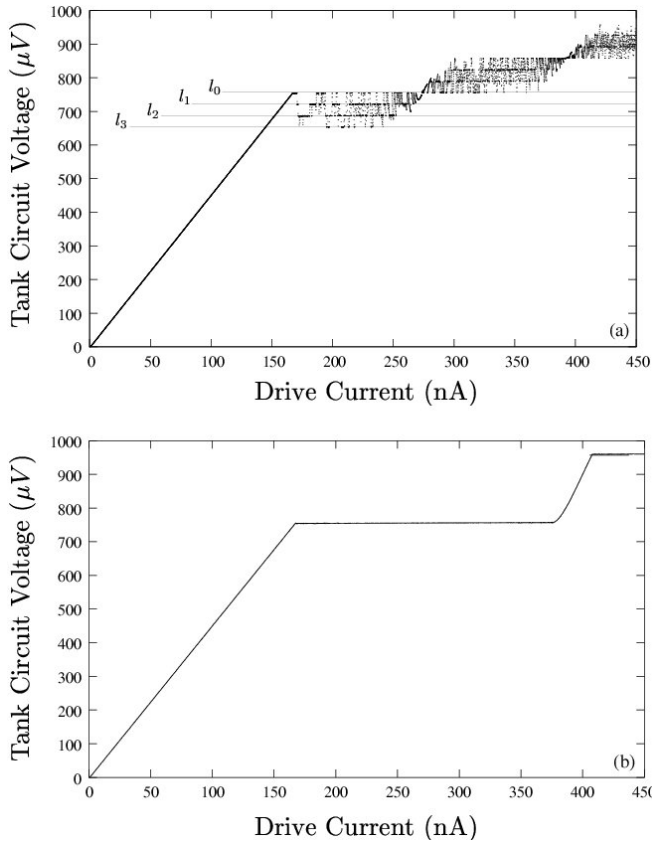


FIG. 2: Dynamic rf voltage (V_{out}) versus rf current (I_{in}) characteristics for a highly hysteretic ($\beta = 137$) SQUID ring-tank circuit system with circuit parameters ring: $C_{sq} = 1 \cdot 10^{13}$ F, $L_{sq} = 6 \cdot 10^{10}$ H, $R_{sq} = 10 \mu\Omega$, $I_c = 75.2$ A; tank circuit: $C_{tc} = 7.6 \cdot 10^{10}$ F, $L_{tc} = 63$ nH and $\beta = M^2 = L_{tc} / L_{sq} = 0.0087$, a bare tank circuit resonant frequency 23 MHz and $\phi_x = 0.0 \phi_0$ (modulus ϕ_0 , n integer).

II. SQUID RING-TANK CIRCUIT DYNAMICS IN THE HIGHLY HYSTERETIC REGIME

With access to more computational power we considered it important to establish the origin of the stochastic jumping in the computer simulations as previously published [1]. As an example of the possible origin of this jumping phenomenon we computed the V_{out} versus I_{in} characteristics for a SQUID ring-tank circuit in the large regime. In this we chose suitable ring and tank circuit parameters for this regime, specially for the SQUID ring: $L_{sq} = 6 \cdot 10^{10}$ H, $I_c = 75.2$ A ($\beta = 137$), $C_s = 10^{13}$ F, $R_s = 10 \mu\Omega$ and for the tank circuit: $C_{tc} = 7.6 \cdot 10^{10}$ F, $L_{tc} = 63$ nH and a quality factor Q of 500, the latter parameters yielding a bare (uncoupled to the ring) tank circuit resonant frequency of 23 MHz. We also set $\beta = M^2 = L_{tc} / L_{sq} = 0.0087$, a coupling quite typical of low noise SQUID ring-tank circuit systems. These are the circuit parameters used throughout this paper. In figure 2 we show two sets of computed V_{out} versus I_{in} characteristics using these ring and tank

circuit parameters. With these values of R_s and C_s the SQUID is underdamped. The originally reported characteristic [1], calculated at relatively low accuracy using a fourth order Runge-Kutta numerical integration routine with an adaptive step size algorithm, is plotted in figure 2 (a) for the first plateau region. In generating this characteristic 4.2 Kelvin current noise, with a thermal noise distribution, has been introduced and the bias flux has been set at $\phi_x = 0.0 \phi_0$ (modulus ϕ_0). Here, the multi-step solutions on the first plateau, and the stochastic jumping between these, are perfectly clear. Since the initial calculations were performed, we have had access to much greater computational power and this has allowed us to apply significantly higher accuracy to our numerical integration. Subsequently we have found that this greatly improved accuracy leads to the suppression of the jumps between the multiple levels in the V_{out} versus I_{in} characteristics. This is very apparent in the other solution shown in figure 2 (b) for which we used exactly the same SQUID and tank circuit parameters as in the characteristic of figure 2 (a). This second solution implies that the experimentally observed jumps may be driven by noise processes but not through current noise as we previously thought. Within the circuit model we have adopted, the alternative is that the driving force arises from some form of voltage perturbation. In order to investigate this possibility we present a number of simulations of the response of this system to voltage pulses applied to the SQUID ring.

In considering the dynamical basis for the plateaux (and the step levels) it is helpful to examine the way in which the SQUID ring flux (ϕ_s) changes in time with the rf drive current (I_{in}). Such a response, is shown in figure 3 for a maximum (sinusoidal) drive flux in the tank circuit of $13.5 \phi_0$ peak to peak (equivalent to a drive flux in the SQUID ring of $0.1175 \phi_0$). In this figure the SQUID ring flux is normalised to ϕ_0 and the time axis is plotted in units of the reciprocal tank circuit period

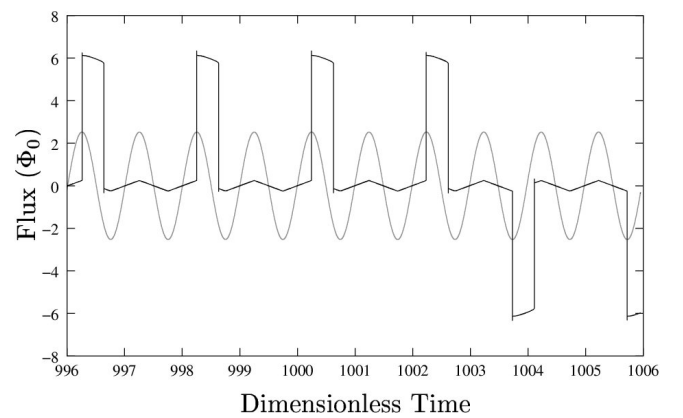


FIG. 3: Time dependence of the normalised SQUID ring flux $\phi_s = \phi_0$ as a function of time, normalised to the tank circuit period $2\pi / L_{tc} C_{tc}$.

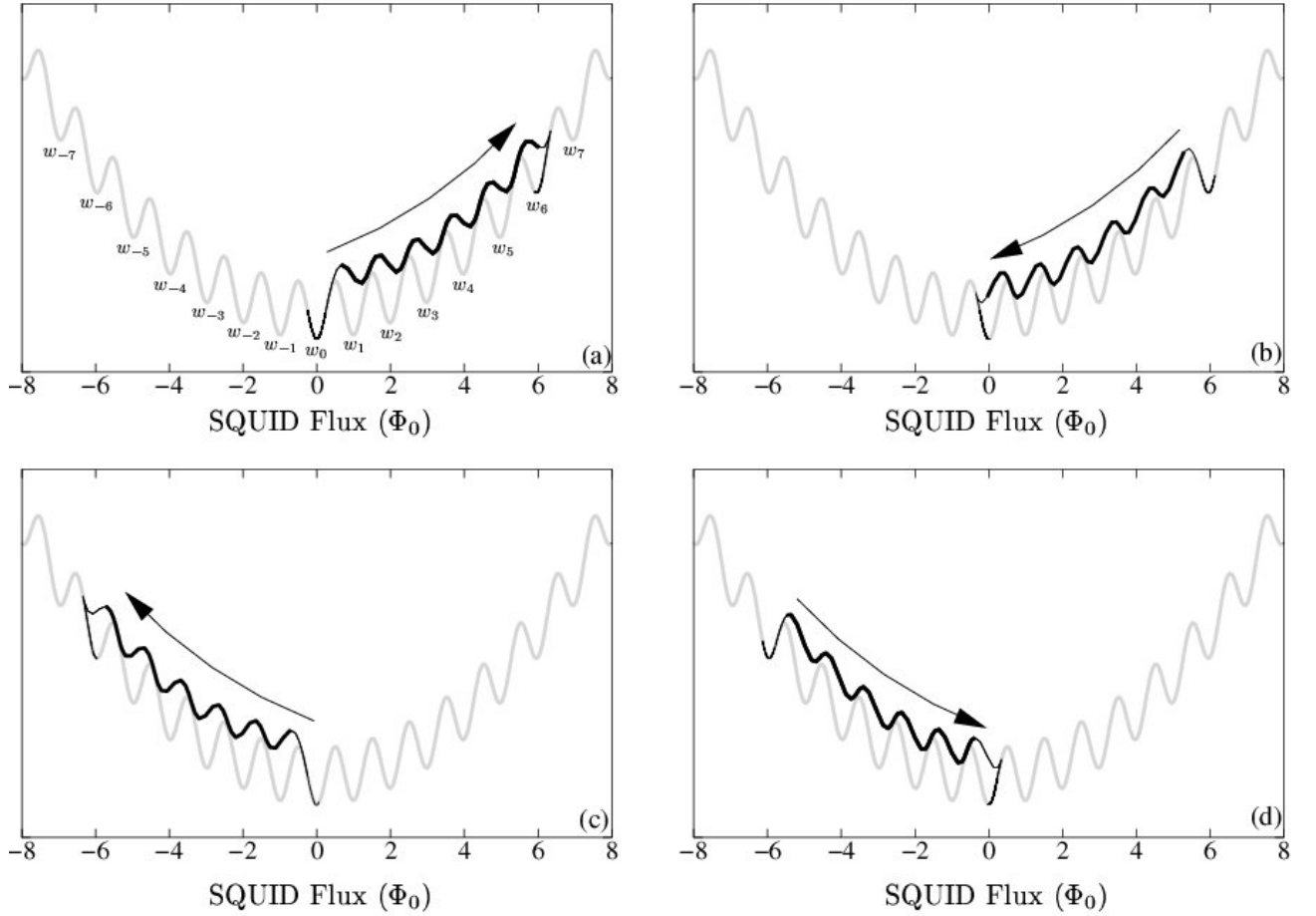


FIG. 4: The SQUID ring potential for the system is shown in grey for (a) a positive s going, outward, multi- Φ_0 trajectory; (b) return trajectory for (a); (c) a negative going, multi- Φ_0 trajectory; (d) return trajectory for (c).

$2 \frac{P}{L_{tc} C_{tc}}$ and, for comparative timing purposes, we show the form of I_{in} in light grey. What this computed plot demonstrates is that, for the most part, the oscillating flux (s) in the underdamped SQUID ring corresponds to the ring being confined to a single well. In figure 3 this single well SQUID ring flux response is shown oscillating over small amplitudes around $s = \Phi_0 = 0$. However, when the drive current reaches maximum amplitude it is found that the SQUID ring can move outside the confines of a single well and make more extended trajectories in the potential (1), i.e. the flux in the ring can jump non-locally (and non-adiabatically) several Φ_0 in s -space between initial and final (target) wells [17]. We now provide some illustrative examples of stable solutions of equations (2) and (3) which give rise to the different voltage levels seen in figure 2 (a).

In the particular example of figure 3 these non-local jumps take place over six wells in s -space relative to the lowest energy well in the potential. Transposed to the rf dynamics of the coupled system, each multi- Φ_0 traversal leads to one of the set of plateau step levels in V_{out} versus I_{in} , as exemplified in figure 2. Examples of

these multi- Φ_0 trajectories (jumps) in the SQUID ring potential can be seen in figure 4, again for the system of figure 2. Taking the origin as the lowest well in this potential, the SQUID flux trajectories shown in figures 3 and 4 correspond to the level denoted l_0 in figure 2 (a). If the origin is displaced to the next lowest well in the potential, the V_{out} versus I_{in} characteristic of the coupled system moves down by one level from the original solution. This level is denoted l_1 in the solutions plotted in figure 2 (a). Moving the origin again to the next lowest well repeats the process, i.e. the dynamics now correspond to the level denoted by l_2 in the solutions plotted in figure 2 (a). A gain, moving the origin to the next lowest well generates the level denoted l_3 in figure 2 (a). However, in our example of a 6 Φ_0 excursion this level (l_3), is equivalent to having displaced our origin to the middle well. We find that beyond this central well in the excursion, attempting to localise our trajectory around one of the remaining three wells simply reverses the shift between the levels on the plateau in figure 2 (a), i.e. starting at l_3 and returning to l_0 through levels l_2 and l_1 . To illuminate this discussion, we can examine, for level l_0 ,

the excursions in the potential shown in the figure 4. Starting in the absolute minimum well of the potential at $s = s_0 = 0$, with $x = 0$ (modulo λ_0), the ring can either execute local motion in this well or occasionally move several λ_0 to a target well. With the ring potential plotted in light grey in figure 4, we show by computation in figure 4(a) one such extended trajectory, starting in the lowest well and followed by a positive going trajectory in s . In this example, having reached the target well the ring completes almost half a tank circuit period in this well before returning to its original starting point in s , as shown in figure 4(b). This mirrors the dynamical behaviour shown in the first four jumps of figure 3. It is also important to note that these non-local excursions do not occur every time the rf drive flux reaches its maximum amplitude, although as the amplitude of the rf drive grows this process happens more frequently. Further multi- λ_0 excursions in the ring potential, but now for negative going s , can be seen in figures 4(c) and (d) for the outward and return paths, respectively. These correspond to the last two pulses in figure 3. In general the target well in the SQUID ring is not symmetric about its centre (minimum) and this is seen to affect the lifetime of the ring in this target well, as evidenced in plots presented in figure 3. In essence the consequence of this is that the ring can reach a new traversal (target) point in drive flux before it has completed half a λ_0 period in s . This phenomenon, arising from the localisation in a non-symmetric well in the SQUID ring potential, means that the excursions in s are only made in one direction.

With the details of figure 4 in mind, and as a possible means to navigate the solutions of (2) and (3), we now consider the effect of rapidly changing voltages applied to the SQUID ring. In order to make this relatively simple, and physically transparent, we simulate the application of appropriately shaped voltage pulses to the SQUID ring, and follow the tank circuit voltage (V_{out}) response. In our example we shall now consider positive amplitude trapezoidal voltage pulses (inset in figure 5) with an upper voltage state time duration of 0.01 tank circuit periods which is activated during the flux traversal shown in bold in figure 4(d). We found that it was only within such highlighted activation regions that the system could be made to respond to these voltage pulses, leading to a level change in V_{out} . For reference we term pulses with positive amplitude as A-type pulse and, conversely, negative amplitude pulses are denoted as B-type. In figure 5 we have plotted the computed tank circuit voltage response as a function of normalised tank circuit time (i.e. in terms of the tank circuit period) for the rf drive amplitude ($I_{in} = 222nA$) set in the middle of the first plateau for the level denoted \downarrow in figure 2(a). In this calculation there was no extraneous flux or voltage noise present and the system was allowed to reach a steady state within this plateau (we note that the initial sharp rise at the beginning of the voltage dynamics is due to transient behaviour). However, after a set time, denoted A_i in figure 5, a voltage pulse of the form shown inset

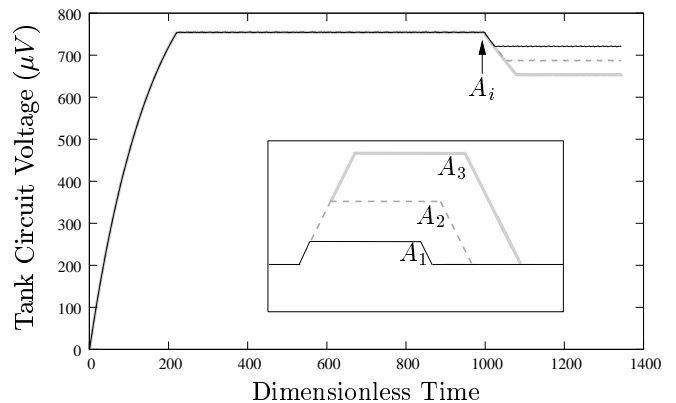


FIG. 5: V_{out} versus normalised time characteristics for the SQUID ring-tank circuit system of figure 2 showing the controlled step to step jumping which can be induced using suitably configured positive (A-type) ramp pulses in the absence of extraneous voltage noise; here we show the effect of increasing the ramp amplitude to induce jumps over one, two or three step intervals.

in this figure was applied. Here, the amplitudes of the pulses $A_i; i = 1; 2; 3$ used were 15, 75 and 120 V, respectively. As is demonstrated in figure 5, the application of a single voltage pulse can change the voltage level of our system by one or more levels at a time, as summarised in table I. If the noiseless (or, in practice, a low enough

Pulse Type	Lower Bound	Upper Bound	Value Used
A_1	15	55	15
A_2	56	90	75
A_3	91	126	120

TABLE I: Summary of pulse amplitude ranges (V) as described in the text.

voltage noise) situation can be realised experimentally, the computational results of figure 5 indicate that multi-level logic, based on SQUID ring-resonator systems could be a feasible proposition. If so, it is reasonable to assume that other forms of voltage pulse could be used for this purposes. With regard to our example, we note that the number of levels on the plateaux depends on the ring parameter values. In the example of figure 5 this is four but could be significantly larger. To further illustrate the control possible we show in figure 6 the result of applying two A-type pulses, in time sequence, to the SQUID ring-tank circuit system.

Of course, the activation pulse in voltage can be negative (B-type) as well as positive. The effect of using such a pulse after an A-type pulse is shown in figure 7 with the form of the B-type pulse shown explicitly in the inset of this figure. This shows that in the absence of extraneous noise, and by a suitable choice of voltage pulse form, we can move at will between the steps on any particular plateau in V_{out} versus I_{in} . To demonstrate that we can

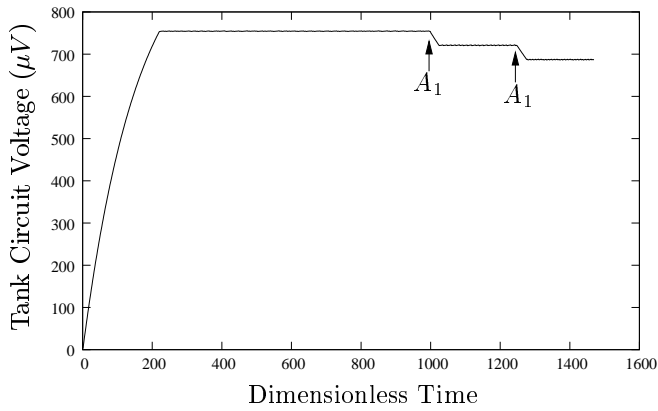


FIG. 6: V_{out} versus normalised time characteristics for the SQUID ring-tank circuit system of figure 2 showing the effect of two sequential A-type voltage pulses in the absence of extraneous voltage noise; as is apparent these step jumps can be induced in a controlled manner.

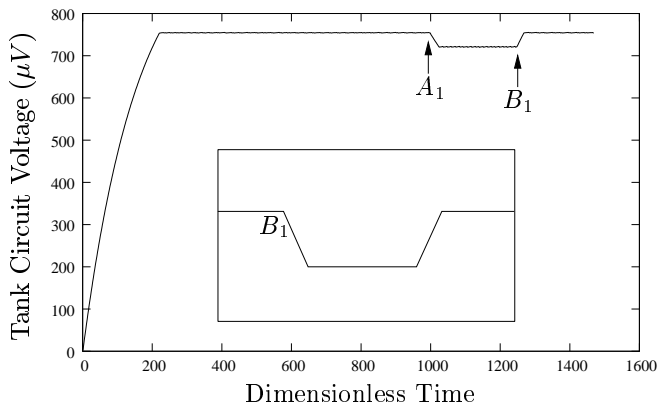


FIG. 7: V_{out} versus normalised time characteristics for the SQUID ring-tank circuit system of figure 2 in the absence of extraneous voltage noise showing the effect of applying sequential A and B-type voltage ramps.

induce step to step jumping at essentially any time of our choosing, we show in figure 8 a sequence of jumps induced by a sequence of A-type pulses spaced by different time intervals. We note that the application of the last pulse causes the tank circuit voltage to step up rather than down.

The computed solutions of figures 5 to 8 show very well the level to level jumping induced by various pulse sequences applied to a highly hysteretic (large β) SQUID ring-tank circuit system. These solutions, which are the end result of very non-linear interactions between the ring and the tank circuit, may be appreciated more clearly by the following qualitative argument. As regards the jumping process between levels on any particular plateau in V_{out} versus I_{in} , the system operates cyclically from an initial (local) well in the SQUID potential (for example the w_0 well in the potential of figure 4). This is shown di-

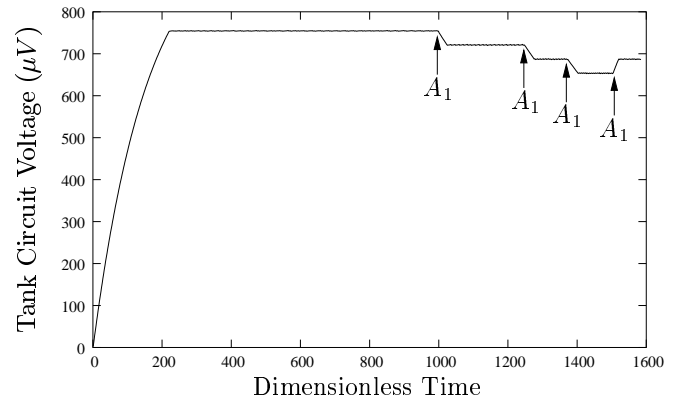


FIG. 8: V_{out} versus normalised time characteristics for the SQUID ring-tank circuit system of figure 2 in the absence of extraneous voltage noise showing the effect of applying sequentially at differing time intervals a set A-type voltage ramps.

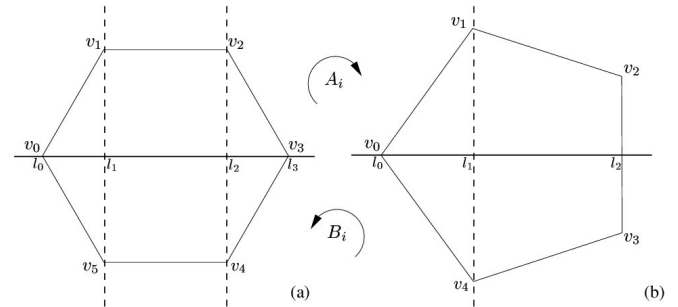


FIG. 9: Graphical representation in the manner in which the wells in the SQUID potential correspond to voltage levels in the V_{out} versus I_{in} characteristic of a highly hysteretic SQUID ring-tank circuit system. The vertices around the polygons indicate which well (in a six well example – see figure 4) the SQUID oscillation is localised in, whilst the letters on the projection denote which one of the set of levels on a particular plateau in V_{out} versus I_{in} the coupled system occupies. See text for more details.

agrammatically in figure 9. The way in which movement between wells in the SQUID potential relates to a given voltage level within a particular plateau can be determined by thinking of each well being mapped on to one of the vertices of a polygon (where the order of the polygon is dependent on the parameter values of the ring-tank circuit system under investigation). This is illustrated in figure 9 (a) for the system considered throughout this paper with the vertices labelled v_i for $i = 0, \dots, 5$ and where the mapping is applied cyclically from the lowest (reference) well of the potential on to each vertex (for our example using the labels for the wells w_i in figure 4 (a) we have the mapping $w_i \rightarrow v_{i \bmod 6}$ for $i \in \mathbb{Z}$). Here, we can find the particular tank circuit voltage level associated with each vertex by projection on to the horizontal axis. For example, the vertices v_1 and v_5 correspond to having

the SQUID ring-tank circuit system in level₁ in figure 2. Clearly, therefore, if the system is moved through an appropriate number of wells it will return to the same state of operation in which it began.

Using this graphical map as the guide, in this paper we have investigated a system with 4 levels, corresponding to figure 9(a). We note that in this example the system must traverse 6 wells in the potential before it returns to its original state of operation. If we choose different SQUID parameters the system can access a variable number of wells within its cycle of operation. However, the system will always display a symmetry about the horizontal axis. For comparison, we show in figure 9(b) a diagram illustrating the situation where the ring-tank circuit system traverses an odd number of wells in the SQUID potential, in this case ve.

By the application of suitable voltage pulses the system can be moved around the vertices of the polygon, so translating the SQUID ring from one potential well to another. Thus, in figure 9(a) application of positive (A-type) pulses causes the ring to move around the polygon in a clockwise direction, whilst negative (B-type) pulses lead to anti-clockwise movement. This movement around the polygon can be performed utilising nearest neighbour, single well, translations, or by multi-₀ traversals between non-local wells in the potential, depending on the magnitude of the applied pulse. The actual level in V_{out} versus I_{in} into which the system settles is determined by three factors: (i) the well in which the SQUID ring is currently localised (ii) the size of voltage pulse used to change location in the potential and (iii) the direction of traversal of the polygon (whether A or B-type pulses are utilised).

III. CONCLUSIONS

In this work we have demonstrated that, in principle, it is possible to use highly hysteretic (large γ) SQUID ring-

tank circuit systems as the basis for multi-level logic or memory devices [18, 19, 20, 21, 22]. Following earlier experiments, where giant SQUID magnetometer plateaux were observed containing sets of constant voltage (V_{out}) steps, we have shown that the jumping processes between steps on a particular plateau can be generated by voltage pulses applied to the system. In the absence of noise (in our computational modelling achieved by the use of high accuracy numerical integration techniques), we find that a high SQUID ring-tank circuit system can remain stably on one of the steps on any particular plateau until a suitably shaped voltage pulse is applied to the ring. Following such a pulse, the ring can be made to jump in a controlled manner to other steps at different levels of V_{out} . This new level can be either above or below the original voltage level, depending on the present state of the system and the type of pulse used. Provided it is possible to reduce the ambient voltage noise on the SQUID ring sufficiently, for example by the use of cryogenically cooled GaAs FET [1] or HEMT-based pre-amplifier electronics [23], it should prove possible to develop devices with a controlled voltage response which can be selected, and modified, at will. This could prove useful in such areas as multi-level logic or finite state machines [18, 19, 20, 21, 22]. As part of any such developments we would expect to see interesting new fields open up in the non-linear dynamics of these highly hysteretic systems.

IV. ACKNOWLEDGEMENTS

We would like to thank the Engineering and Physical Sciences Research Council for its generous support of this work. We would also like to thank Dr. R.J. Prance and Professor A.R. Bulsara for interesting and informative discussions.

-
- [1] R. J. Prance, R. W. Hiteman, T. D. Clark, H. Prance, V. Scholmann, J. F. Ralph, S. Alkhwaja, and M. Everitt, *Phys. Rev. Lett.* 82, 5401 (1999).
 - [2] J. R. Friedman, V. Patel, W. Chen, S. K. Tolpygo, and J. E. Lukens, *Nature* 406, 43 (2000).
 - [3] C. H. van der Wal, A. C. J. ter Haar, F. K. Wilhelm, R. N. Schouten, C. J. P. M. Hamans, T. P. Orlando, S. Llyd, and J. E. Mooij, *Science* 290, 773 (2000).
 - [4] T. P. Spiller, *Fortschritte Phys.-Prog. Phys.* 48, 1075 (2000).
 - [5] I. Chiorescu, Y. Nakamura, C. J. P. M. Hamans, and J. E. Mooij, *Science* 299, 1869 (2003).
 - [6] W. C. Schieve, A. R. Bulsara, and E. W. Jacobs, *Phys. Rev. A* 37, 3541 (1988).
 - [7] M. P. Soerensen, M. Bartuccelli, P. L. Christiansen, and A. R. Bishop, *Phys. Lett. A* 109, 347 (1985).
 - [8] K. Likharev, *Dynamics of Josephson Junctions and Circuits* (Taylor & Francis, 1986).
 - [9] L. Chua, C. Desoer, and E. Kuh, *Linear and Non-Linear Circuits* (McGraw-Hill, 1987).
 - [10] A. Barone and G. Paterno, *Physics and Applications of the Josephson Effect* (John Wiley & Sons Inc., 1982).
 - [11] T. D. Clark, J. F. Ralph, R. J. Prance, H. Prance, J. Diggs, and R. W. Hiteman, *Phys. Rev. E* 57, 4035 (1998).
 - [12] O. Lounasmaa, *Experimental Principles and Methods below 1K* (Academic Press, 1974).
 - [13] J. Zimmerman, P. Thiene, and J. Harding, *J. Appl. Phys.* 41 (4), 1572 (1970).
 - [14] L. Gamaitoni, P. Hanggi, P. Jung, and F. Marchesoni, *Rev. Mod. Phys.* 70, 223 (1998).
 - [15] A. R. Bulsara and L. Gamaitoni, *Phys. Today* 49, 39 (1996).

- [16] J.F. Lindner, J. Mason, J. Neugebauer, B.J. Breen, W.L. Ditto, and A.R. Bulsara, *Phys. Rev. E* 63 (4), 041107 (2001).
- [17] E. Ben Jacob and D. Abraham, *Appl. Phys. Lett.* 39, 835 (1981).
- [18] R.K. Brayton, G.D. Hachtel, and A.L. Sangiovanni-Vincentelli, *Proc. IEEE* 78, 264 (1990).
- [19] S. Devadas, H.K. Ma, A.R. Newton, and A. Sangiovanni-Vincentelli, *IEEE Trans. Comput-Aided Des. Integr. Circuits Syst.* 7, 1290 (1988).
- [20] K. Bartlett, W. Cohen, A. Degeus, and G. Hachtel, *IEEE Trans. Comput-Aided Des. Integr. Circuits Syst.* 5, 582 (1986).
- [21] B. Lin and S. Devadas, *IEEE Trans. Comput-Aided Des. Integr. Circuits Syst.* 14, 974 (1995).
- [22] R. Li, J. Wang, Y. Wang, W. Dong, and W. D. X., 1998 5th International Conference On Solid-State And Integrated Circuit Technology Proceedings pp. 588-589 (1998).
- [23] C. Boutez, P. Crozat, V. Danelon, M. Chaubet, P. Febvre, and G. Beaudin, *Int. J. Infrared Millimeter Waves* 18, 85 (1997).